THE EFFECT OF THERMOPHYSICAL PROPERTIES ON NONLINEAR THERMAL-SOLUTAL CONVECTIVE FLOW OF CASSON NANOFLUID OVER AN INCLINED SURFACE WITH HIGHER ORDER CHEMICAL REACTION

Timothy Lanre Oyekunle[1*], Mojeed Taiwo Akolade[1], Samson Ademola Agunbiade[2]

[1] Department of Mathematics, University of Ilorin, Ilorin, Nigeria
   e-mail: tloyekunle95@gmail.com, akolademojeed@yahoo.com
[2] Department of Basic Sciences, Babcock University, Ogun State, Nigeria
   e-mail: agunbiade1971@gmail.com
corresponding author

Abstract

The combined effect of Soret-Dufour, higher-order chemical reaction and variable thermophysical properties on nonlinear thermal and solutal convective flow of a non-Newtonian fluid (Casson nanofluid) over a slanted surface is analyzed. The nonlinear dimensionless equations governing the fluid flow are transformed into ordinary differential equations, using suitable similarity transformation variables. The flow fields and some characteristic numerical results are obtained from these equations, using collocation method with assumed Legendre functions of the first kind. These results are presented in the form of graphs and tables showing the impact of various parameters on the fluid flow, heat and mass characteristics. It is observed that a rise in chemical reaction parameter decreases the nanoparticle volume fraction while a higher order of chemical reaction makes it elevated. The velocity increases and temperature decreases with a rise in nonlinear thermal convection and higher value of nonlinear solutal convection has effect on the rise of velocity distribution.

Keywords: Casson nanofluid, thermophysical properties, chemical reaction, Legendre polynomial, inclined surface.

1. Introduction

In the simultaneous occurrence of heat and mass transfer, with chemical reaction, the presence of foreign mass in water or air produces a type of chemical reaction which may either be presented naturally or mixed with water or air. Chemical reaction may either be homogeneous or heterogeneous in nature. When the reaction rate is directly proportional to the nth power of species concentration, it is said to be of order n (Hayat et al., 2011). The practical consequence is enormous in many branches of sciences and engineering. They are being used in the formation of new compounds from raw materials such as mineral ores, petroleum and thermite reaction to generate light and heat in pyrotechnics and wedding. (Loganathan et al., 2011). Casson nanofluid has gained increasing attention due to its applications in naturally occurring processes and industries involving fluid flow. Some of its applications are seen in cosmetic, pharmaceutical and

chemical industries in the manufacturing of china clay, paints, syrups, gas, juice, cleanser, chemicals, etc. (Chaoyang et al., 1989 and Jawad et al., 2016).

These diverse applications encouraged researchers such as Gupta et al. (2018) to examine the impact of chemical reaction and radiation on mixed convective MHD stagnation point flow and heat transfer of nanofluid on a slanted stretching sheet. Gbadeyan et al. (2018) studied the effects of Dufour, Soret and chemical reaction with MHD flow on heat and mass transfer through a wavy channel. It was discovered that velocity and concentration accelerated with chemical reaction while temperature reversed the case. The nth order chemical reaction flow through an unsteady nano-bioconvective channel was studied by Faisal et al. (2021). They pointed out that mass transfer rate at the upper wall decreased and that of the lower wall increased with the destructive second order chemical reaction. Buongiorno (2006) investigated the convective transport in a nanofluid. Animasaun (2015) looked into the effects of thermophysical properties with nth order chemical reaction and suction on heat and mass transfer of non-darcian MHD dissipative Casson fluid. Oyekunle et al. (2021) examined the effects of Soret, Dufour and dissipation with chemical reaction on heat and mass transfer of MHD Casson nanofluid. It was recorded that a larger value of chemical reaction accelerated the velocity and reduced the concentration profiles. The impact of radiation and chemical reaction on unsteady MHD flow of nanofluid over a stretching sheet was investigated by Daniel et al. (2017).

Thermophysical properties are very important and sensitive when it comes to rises in the temperature of the fluid. It causes a significant change in the fluid physical properties, especially in the lubrication theory which is usually affected by the increase in the temperature and heat generated from internal friction (Jawali and Chamkha, 2015, Akolade et al. 2021a). Unstable viscosity caused by variation in temperature is applicable in engineering and environmental when turbulent flow is encountered.

These applications motivated researchers such as Jawali and Chamkha (2015) who registered the effects of variable viscosity and thermal conductivity on free convective viscous fluid flow through a vertical channel. It is noticed that the fluid flow and heat transfer accelerate with an increase in variable viscosity while the reverse is the case with a rise in variable thermal conductivity. The influence of thermophysical properties with convective heating and velocity slip on Casson nanofluid is analyzed by Gbadeyan et al. (2020). They discovered that fluid flow is enhanced while temperature and concentration decrease with a rise in the variable properties. The influence of the variable properties with Soret-Dufour on non-Newtonian fluid flow over a vertical porous plate is investigated by Idowu et al. (2020). The influence of variable properties on fluid flow through different geometries has also gained the attention of other researchers such as Salawu and Dada (2016), Malik et al. (2016), Shah et al. (2018), Hayat et al. (2016) and Umavathi et al. (2017).

Due to the applications of nonlinear thermal and solutal convective flow, as stated by (Patil and Kulkami, 2019) that it is useful when operating with high temperature in the field of engineering, sciences and industries, researchers Raju et al. (2017) and Raju et al. (2018) analyzed the effect of quadratic convection with time dependency and Darcy porous medium, respectively, on Casson fluid flow through the same geometry. They registered that higher value of quadratic convection increases the momentum of the fluid particles. Idowu et al. (2021) and Akolade el al. (2021b) analyzed the impacts of quadratic convection on MHD Casson fluid flow through different geometries. They recorded that a hike in nonlinear convection accelerates both velocity and temperature, while a reduction is noticed in concentration fields. Kumar and Sood (2016) observed that the flow fields are enhanced with a hike in nonlinear convection parameters in the study of the effects of quadratic convection on stagnation point of two-dimensional boundary layer flow over a shrinking sheet. Nagaendramma et al. (2018), Upadhya et al. (2018a), Upadhya

et al. (2018b), Ibrahim et al. (2017) among others also showed their interest in the impacts of nonlinear convection on fluid flow through different geometries.

The analysis of the effects of variable thermophysical properties on nonlinear thermal and solutal convective flow of Casson nanofluid on a sloped surface with higher order chemical reaction is the focus of this paper. To the best of the authors' knowledge, no attention has been given to this kind of research in the literature. The dimensional governing equations of the fluid flow are nondimensionalized and transformed to ordinary differential equations. In section 2, the model formulation and controlling systems of equation governing the flow system is discussed. In section 3, collocation method with the aid of assumed Legendre functions of the first kind and MATHEMATICAL 11.0 software is employed. Results of the emerging parameters are elucidated in section 4 while conclusions are drawn in section 5.

2. Problem formulation

An incompressible, two dimensional, laminal, steady, hydromagnetic Casson nanofluid flow with nonlinear convective and higher order chemical reaction is examined. The direction of the fluid flow parallel to the plate is taken as $\bar{x}$ -axis, while $\bar{y}$ -axis is taken perpendicular to it as shown in the physical geometry of the flow (Fig. 1). The induced magnetic field is negligible, as it is assumed very small compared to the applied magnetic field. Hence, there is application of variable magnetic field $B(\bar{x}) = B_0 / \sqrt{\bar{x}}$ and electrical field effect $\sigma = \sigma_0 \bar{u}$ normal to the slanted plate, where B_0, σ_0 are the constant magnetic and electrical field, respectively. T_f and T_∞ are taken to be surface of the plate and ambient temperature while C_w and C_∞ are taken to be wall and ambient mass transfer, respectively.
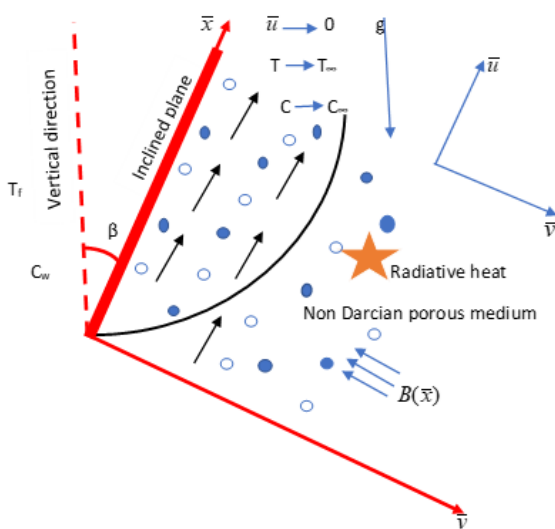
Fig. 1. Physical geometry of the flow.

From the assumptions stated above and the theory of the usual Boussinesq approximation, the fluid flow governing equations are (Oyekunle et al., 2021, Akolade et al., 2021a and Uddin et al., 2012).

$$\frac{\partial \overline{u}}{\partial \overline{x}} + \frac{\partial \overline{v}}{\partial \overline{y}} = 0, \tag{1}$$

$$\rho_f \, (\overline{u} \, \frac{\partial \overline{u}}{\partial \overline{x}} + \overline{v} \, \frac{\partial \overline{v}}{\partial \overline{y}}) = (1 - \alpha^{-1}) \frac{\partial}{\partial \overline{y}} [\mu(T) \frac{\partial \overline{u}}{\partial \overline{y}}] + g\cos \beta [\Lambda_0 (T - T_\infty) + \Lambda_1 (T - T_\infty)^2 +$$

$$\Lambda_2 (C - C_\infty) + \Lambda_3 (C - C_\infty)^2] - \sigma_0 B^2 (\overline{x}) \overline{u}^2 - \frac{\mu_b (T)(1 + \alpha^{-1})}{k_p} \overline{u} - \frac{b^*}{k_p} \overline{u}^2, \tag{2}$$

$$\overline{u} \, \frac{\partial T}{\partial \overline{x}} + \overline{v} \, \frac{\partial T}{\partial \overline{y}} = \frac{1}{\rho_f c_p} \frac{\partial}{\partial \overline{y}} [k(T) \frac{\partial T}{\partial \overline{y}}] + \tau [D_B \frac{\partial C}{\partial \overline{y}} \frac{\partial T}{\partial \overline{y}} + \frac{D_T}{T_\infty} (\frac{\partial T}{\partial \overline{y}})^2] - \frac{1}{\rho_f c_p} \frac{\partial q_r}{\partial \overline{y}} +$$

$$\frac{Q_1 (T - T_\infty)}{\rho_f c_p} + \frac{D_m k_0}{c_s c_p} \frac{\partial^2 C}{\partial \overline{y}^2} + \frac{\mu_b (T)(1 + \alpha^{-1})}{\rho_f c_p} (\frac{\partial \overline{u}}{\partial \overline{y}})^2, \tag{3}$$

$$\overline{u} \, \frac{\partial C}{\partial \overline{x}} + \overline{v} \, \frac{\partial C}{\partial \overline{y}} = D_B \frac{\partial^2 C}{\partial \overline{y}^2} + \frac{D_T}{T_\infty} \frac{\partial^2 T}{\partial \overline{y}^2} + \frac{D_m k_0}{T_m} \frac{\partial^2 T}{\partial \overline{y}^2} - k(C - C_\infty)^n, \tag{4}$$

The conditions of the boundary are

$$\overline{u} = u_{slip}, \quad -k(T) \frac{\partial T}{\partial \overline{y}} = h_f (\overline{x})(T_f - T), \quad\quad C = C_w \quad\quad at \quad\quad \overline{y} = 0,$$

$$\overline{u} = 0, \quad T \to T_\infty, \quad\quad C \to C_\infty \quad\quad as \quad\quad \overline{y} \to \infty, \tag{5}$$

The radiative heat flux, using Rossland approximation for diffusion is defined as

$$q_r = \frac{4\sigma_1}{3k_1} \frac{\partial T^4}{\partial \overline{y}}, \tag{6}$$

where σ_1 and k_1 are the Stefan-Boltzmann number and Rossland absorption constant, respectively. $T^4 = 4T_\infty^3 T - 3T_\infty^4$.

Following, Idowu & Falodun (2020) and Akolade et al. (2021a), the thermal conductivity and viscosity are taken as

$$\mu(T) = \mu_0 [1 + a_1 (T_w - T)], \quad \kappa(T) = \kappa_0 [1 + a_2 (T - T_\infty)], \quad u_{slip} = S_1 \frac{\mu_b (T)(1 + \alpha^{-1})}{\rho_f} \frac{\partial \overline{u}}{\partial \overline{y}}, \tag{7}$$

Introducing the following non-dimensional variables into equations (1)-(5) gives the equations in a dimensionless form.

$$x = \frac{\overline{x}}{L}, \quad y = \frac{\overline{y} \sqrt[4]{Ra}}{L}, \quad u = \frac{\overline{u} L}{\alpha^* \sqrt{Ra}}, \quad v = \frac{\overline{v} L}{\alpha^* \sqrt[4]{Ra}}, \quad \Phi = \frac{C - C_\infty}{C_w - C_\infty}, \quad \Theta = \frac{T - T_\infty}{T_f - T_\infty}, \tag{8}$$

The equations are

$$\frac{\partial u}{\partial x} + \frac{\partial v}{\partial y} = 0, \tag{9}$$

$$u\frac{\partial u}{\partial x}+v\frac{\partial u}{\partial y}=P_r\left(1+\alpha^{-1}\right)\{[1+\gamma_1(1-\Theta)]\left(\frac{\partial^2 u}{\partial y^2}-\frac{L^2}{k_p\sqrt{Ra}}u\right)\}-P_r\left(1+\alpha^{-1}\right)\gamma_1\frac{\partial u}{\partial y}\frac{\partial\Theta}{\partial y}-$$

$$\left(\frac{H}{x}+\frac{b^*L}{k_p}\right)u^2+P_r\cos\beta\left[\left(\Theta+\chi\Theta^2\right)+Nr\left(\Phi+\varepsilon\Phi^2\right)\right],\tag{10}$$

$$u\frac{\partial\Theta}{\partial x}+v\frac{\partial\Theta}{\partial y}=(1+\gamma_2\Theta+R)\frac{\partial^2\Theta}{\partial y^2}+B_r\frac{\partial\Phi}{\partial y}\frac{\partial\Theta}{\partial y}+\{T_m+\gamma_2\}\left(\frac{\partial\Theta}{\partial y}\right)^2+G\Theta+D_f\frac{\partial^2\Phi}{\partial y^2}$$

$$+P_r\frac{\alpha^{*2}Ra}{L^2 C_p(T_f-T_\infty)}\{1+\gamma_1(1-\Theta)\}\left(1+\alpha^{-1}\right)\left(\frac{\partial u}{\partial y}\right)^2,\tag{11}$$

$$u\frac{\partial\Phi}{\partial x}+v\frac{\partial\Phi}{\partial y}=\left(\frac{T_m}{B_r}\frac{1}{L_e}+S_r\right)\frac{\partial^2\Theta}{\partial y^2}+\frac{1}{L_e}\frac{\partial^2\Phi}{\partial y^2}-\gamma\Phi^n,\tag{12}$$

With the boundary conditions

$$\left.\begin{array}{l}u=S\{1+\gamma_1(1-\Theta)\}\left(1+\frac{1}{\alpha}\right)\frac{\partial u}{\partial y},\quad v=0,\quad\frac{\partial\Theta}{\partial y}=-\frac{Bi(1-\Theta)}{(1+\gamma_2\Theta)},\quad\Phi=1\ at\ y=0,\\ u\to 0,\qquad\qquad\Theta\to 0,\qquad\Phi\to 0,\qquad\qquad as\ y\to\infty.\end{array}\right\},\tag{13}$$

where,

$$Sr=\frac{D_m k_0(T_f-T_\infty)}{T_m\alpha^*(C_w-C_\infty)},R=\frac{16\sigma_1 T_\infty^3}{3k_1 k},N_r=\frac{\Lambda_2(C_w-C_\infty)}{\Lambda_0(T_w-T_\infty)},Ra=\frac{g\Lambda_0 L^3(T_f-T_\infty)}{\alpha^*\upsilon},H=\frac{\sigma_0 B_0^2}{\rho_f}$$

$$\gamma_1=a_1(T_f-T_\infty),\ \gamma_2=a_2(T_f-T_\infty),\chi=\frac{\Lambda_1}{\Lambda_0}(T_f-T_\infty),\varepsilon=\frac{\Lambda_3}{\Lambda_2}(C_w-C_\infty),P_r=\frac{\upsilon}{\alpha^*},$$

$$B_r=\frac{\tau D_B(C_w-C_\infty)}{\alpha^*},T_m=\frac{\tau D_T(T_f-T_\infty)}{\alpha^* T_\infty},G=\frac{L^2 Q_1}{\alpha^*\rho_f c_p\sqrt{Ra}},D_f=\frac{D_m k_0(C_w-C_\infty)}{T_m\alpha^* c_s c_p(T_f-T_\infty)},\tag{14}$$

$$L_e=\frac{\alpha^*}{D_B},\gamma=\frac{kL^2(C_w-C_\infty)^{n-1}}{\alpha^*\sqrt{Ra}},S=\frac{s_1\mu_0\sqrt[4]{Ra}}{\rho_f L},\quad Bi=\frac{Lh_f(x)}{k_0\sqrt[4]{Ra}}.$$

The representation of each parameter in equation (14) is as stated in the nomenclature.

The Stream function is taken as

$$u=\frac{\partial\psi}{\partial y},\qquad v=-\frac{\partial\psi}{\partial x},\tag{15}$$

Introducing equation (15) into equations (9)-(13), equation (9) is identically satisfied while equations (10)-(13) become

$$\frac{\partial\psi}{\partial y}\frac{\partial^2\psi}{\partial x\partial y}-\frac{\partial\psi}{\partial x}\frac{\partial^2\psi}{\partial y^2}=P_r\left(1+\alpha^{-1}\right)\{1+\gamma_1(1-\Theta)\}\left[\frac{\partial^3\psi}{\partial y^3}-\frac{L^2}{k_p\sqrt{Ra}}\frac{\partial\psi}{\partial y}\right]+\left\{\frac{H}{x}+\frac{b^*L}{k_p}\right\}\left(\frac{\partial\psi}{\partial y}\right)^2$$

$$-P_r\left(1+\alpha^{-1}\right)\gamma_1\frac{\partial\Theta}{\partial y}\frac{\partial^2\psi}{\partial y^2}+P_r\cos\beta\left[\left(\Theta+\chi\Theta^2\right)+Nr\left(\Phi+\varepsilon\Phi^2\right)\right],\tag{16}$$

$$\frac{\partial \psi}{\partial y}\frac{\partial \Theta}{\partial x} - \frac{\partial \psi}{\partial x}\frac{\partial \Theta}{\partial y} = \{1+\gamma_2\Theta + R\}\frac{\partial^2\Theta}{\partial y^2} + B_r\frac{\partial \Phi}{\partial y}\frac{\partial \Theta}{\partial y} + \{T_m + \gamma_2\}\left(\frac{\partial \Theta}{\partial y}\right)^2 + G\Theta +$$

$$D_f\frac{\partial^2\Phi}{\partial y^2} + P_r\frac{\alpha^{*2}Ra}{L^2C_p(T_f-T_\infty)}\{1+\gamma_1(1-\Theta)\}\left(1+\alpha^{-1}\right)\left(\frac{\partial^2\psi}{\partial y^2}\right)^2,$$

(17)

$$\frac{\partial \psi}{\partial y}\frac{\partial \Phi}{\partial x} - \frac{\partial \psi}{\partial x}\frac{\partial \Phi}{\partial y} = \frac{1}{L_e}\frac{\partial^2\Phi}{\partial y^2} + \left(\frac{T_m}{B_r}\frac{1}{L_e} + S_r\right)\frac{\partial^2\Theta}{\partial y^2} - \gamma\Phi^n,$$

(18)

With boundary conditions

$$\left.\begin{array}{l}\dfrac{\partial \psi}{\partial y} = \dfrac{s_1\mu_0\sqrt[4]{Ra}}{\rho_f L}\{1+\gamma_1(1-\Theta)\}\left(1+\alpha^{-1}\right)\left(\dfrac{\partial^2\psi}{\partial y^2}\right), \\[3mm] \dfrac{\partial \Theta}{\partial y} = -\dfrac{Lh_f(x)}{k_0\sqrt[4]{Ra}}\dfrac{(1-\Theta)}{(1+\gamma_2\Theta)}, \quad \Theta = 1, \ at \ y = 0 \\[3mm] \dfrac{\partial \psi}{\partial y} \to 0, \ \Theta \to 0, \ \Phi \to 0, \ as \ y \to \infty.\end{array}\right\}.$$

(19)

To transform equations (16)-(19), the following similarity transformations are used.

$$\left.\begin{array}{l}\xi = \dfrac{y}{\sqrt[4]{x}}, \qquad \psi = \sqrt[4]{x^3}\Upsilon(\xi), \qquad \Theta = \Theta(\xi), \ \Phi = \Phi\left(\xi\right) \\[3mm] b^* = \dfrac{1}{\sqrt{x}}(b^*)_0, \qquad k_p = \sqrt{x}(k_p)_0, \qquad h_f(x) = \sqrt[4]{x}(h_f)_0\end{array}\right\},$$

(20)

Introducing equation (20) into equations (16)-(19) gives the following transformed equations

$$\left(1+\alpha^{-1}\right)\{[1+\gamma_1(1-\Theta)]\Upsilon''' - \gamma_1\Upsilon''\Theta'\} + \tfrac{1}{4P_r}\left[3\Upsilon\Upsilon'' - 2\Upsilon'^2 - 4(H+B)\Upsilon'^2\right] +$$

$$\cos\beta\{(\Theta + \chi\Theta^2) + N_r(\Phi + \varepsilon\Phi^2)\} - \tfrac{1}{D_a}\left(1+\alpha^{-1}\right)[1+\gamma_1(1-\Theta)]\Upsilon' = 0,$$

(21)

$$\left(1+\gamma_2\Theta + R\right)\Theta'' + \tfrac{3}{4}\Upsilon\Theta' + B_r\Phi'\Theta' + (\gamma_2 + T_m)\Theta'^2 + G\Theta + D_f\Phi'' +$$

$$P_r Ec\left(1+\alpha^{-1}\right)[1+\gamma_1(1-\Theta)]\Upsilon''^2 = 0,$$

(22)

$$\Phi'' + \tfrac{3}{4}L_e\ \Upsilon\Phi' - L_e\ \gamma\Phi^n + \left(\tfrac{T_m}{B_r} + L_e S_r\right)\Theta'' = 0,$$

(23)

With the boundary conditions

$$\left.\begin{array}{l}\Upsilon'(0) = s[1+\gamma_1(1-\Theta)]\left(1+\alpha^{-1}\right)\Upsilon''(0), \\[2mm] \Upsilon(0) = 0, \ \Theta'(0) = -\dfrac{B_i(1-\Theta(0))}{(1+\gamma_2\Theta)}, \ \Phi(0) = 1, \\[2mm] \Upsilon'(\infty) \to 0, \quad \Theta(\infty) \to 0, \quad \Phi(\infty) \to 0.\end{array}\right\}$$

(24)

where

$$Ec = \frac{\alpha^{*2}Rax^{-1}}{L^2c_p(T_f-T_\infty)}, \quad Da = \frac{(k_p)_0\sqrt{Ra}}{L^2}, \quad B = \frac{(b^*)_0 L}{(k_p)_0}, \quad Bi = \frac{(h_f)_0 L}{k_0\sqrt[4]{Ra}}, \quad S = \frac{s_1\mu_0\sqrt[4]{Ra}}{\rho_f L}, \quad (25)$$

The nomenclature states the representation of each parameter in equation (25).

2.1 *Flow characteristics*

The Nusselt ($Nu_{\bar{x}}$) and Sherwood ($Sh_{\bar{x}}$) are defined as (Uddin et al., 2012)

$$
Nu_{\bar{x}} = -\bar{x}\frac{\left(\dfrac{\partial T}{\partial \bar{y}}\right)_{\bar{y}=0}}{(T_f - T_\infty)}, \qquad Sh_{\bar{x}} = -\bar{x}\frac{\left(\dfrac{\partial C}{\partial \bar{y}}\right)_{\bar{y}=0}}{(C_w - C_\infty)}. \tag{26}
$$

Introducing equations (8), (15) and (20) into equation (26) results in the reduced Nusselt and Sherwood numbers, respectively,

$$
\frac{1}{\sqrt[4]{Ra_{\bar{x}}}}Nu_{\bar{x}} = -\Theta'(0) \quad and \quad \frac{1}{\sqrt[4]{Ra_{\bar{x}}}}Sh_{\bar{x}} = -\Phi'(0). \tag{27}
$$

Where the local Rayleigh number is $Ra_{\bar{x}} = \dfrac{g\lambda_1\left(T_f - T_\infty\right)\bar{x}^3}{\alpha^* v}$.

3. Method of solution

Legendre collocation method with polynomial as the basis function is used to obtain the solution of non-linear, coupled, ordinary differential equations (21)-(24). The domain truncation approach $[0,L]$ is used to truncate the interval $[0,\infty)$. Through the following algebraic mapping:

$$
\eta = \frac{2\xi}{L} - 1, \tag{28}
$$

the interver [0,L] is transformed to [-1,1]. Here, L is the scaling parameter and it is assumed sufficiently large in relative to the boundary layer thickness (Olagunju et al. (2013), Aysun and Salih, (2013)). The sum of a finite series of the legendary polynomial $p_j(\eta)$ is the approximation solution of the function $\Upsilon(\xi)$, $\Theta(\xi)$ and $\Phi(\xi)$, given as

$$
\Upsilon(\xi) \cong \Upsilon_N(\eta) = \sum_{j=0}^{N}a_j p_j(\eta), \ \ \Theta(\xi) \cong \Theta_N(\eta) = \sum_{j=0}^{N}b_j p_j(\eta),
$$
$$
\Phi(\xi) \cong \Phi_N(\eta) = \sum_{j=0}^{N}c_j p_j(\eta), \text{ for } j = 0,1,...,N, \tag{29}
$$

The unknown constants to be determined are a_j , b_j and c_j . The generated equations of $3N+3$ algebraic system with $3N+3$ unknown coefficient is solved, using symbolic package of MATHEMATICA 11.0 with Newton iteration technique. Hence, the unknown constant a_j , b_j and c_j are determined and the flow distributions and characteristic solutions are obtained.

4. Results and Discussion

Using the proposed method to solve equations (21)-(23) with boundary condition (24) for the flow fields and its characteristics, Fig. (2)-(11) depict the graphical representation of the solution for velocity, temperature and concentration, with fixed default values $H=Bi=0.5$, $Pr=6.8$, $Ec=D_f=G=0.01$, $B_r=T_m=B=R=N_r=0.1$, $D_a=10$, $L_e=n=1.0$, $\alpha=\Upsilon_1=\Upsilon_2=S=S_r=0.3$, $\Upsilon=0.2$, $\beta=\pi/6$, $\chi=\varepsilon=1.5$ (Uddin et al. 2012, Oyekunle et al. 2021, Gbadeyan et al. 2020). Table 1 shows the comparison of the Nusselt number of the present work with the work of Uddin et al. (2012) and Gbadeyan et al. (2020), which is found to be in an excellent agreement when the embedded parameters are set to zero. Table 2 presents the computational values of Nusselt and Sherwood numbers for various parameters of interest. The influence of the parameters considered on both Nusselt and Sherwood numbers are as shown in the table.

Figure 2(a, b, c) depicts the effect of thermophoretic parameter (T_m) on the velocity (Υ'), temperature (Θ) and nanoparticle volume fraction (Φ). It is realized that velocity and concentration increased while temperature decreased with a rise in the thermophoretic parameter. The Brownian motion (B_r) impact on velocity, temperature and nanoparticle volume fraction is depicted in Fig. 3 (a, b, c). The figure shows that the velocity and temperature accelerate with Brownian motion, while a reduction in nanoparticle volume fraction is observed due to the interaction of the nanofluid particles that generated thermal energy to increase the fluid temperature.

Fig. 4 presents the effect of viscosity (γ_1) on (a) velocity (b) temperature profiles. The velocity diminished and the temperature elevated with a rise in γ_1. The impact of thermal conductivity (γ_2) on (a) velocity (b) temperature is displayed in Fig. 5. The figure clarifies that the velocity and temperature profiles increase with γ_2. Physically, the thermal boundary layer generates heat due to higher thermal conductivity to elevate the temperature field.

Fig. 6 depicts the influence of the nonlinear thermal convection (χ) on (a) velocity (b) temperature field. The velocity is increases and temperature decreases with an increase in thermal convection. The impact of nonlinear Solutal convection (ε) on the velocity is displayed in Fig. 7(a). It is realized that a hike in the Solutal convection gives a slight increase in velocity profile. Physically, to predict an accurate heat and mass transfer across the flow field for the convection process, thermal conductivity material is required to be upgraded. The influence of nth order chemical reaction (n) on the nanoparticle volume fraction is presented in Fig. 7(b). It is observed that the nanoparticle volume fraction increased with the order of chemical reaction.

Fig. 8 explains the influence of inclination angle (β) on the (a) velocity, (b) temperature and (c) concentration distributions. It is discovered that a rise in β reduces the velocity and accelerates temperature and concentration profiles. In the physical sense, the higher the inclination angles the more the external magnetic field is strengthened. The influence of chemical reaction parameter γ and Soret parameter S_r on nanoparticle volume fraction is shown in Fig. 9(a, b). It is recorded that a higher value of chemical reaction parameter diminished the nanoparticle volume fraction while a larger number of S_r elevated it.

Fig. 10(a, b) depicts the influence of Dufour (D_f) on the velocity and temperature, respectively. The velocity and temperature distributions increase with a higher value of D_f. The energy flux generated due to the larger value of D_f accelerate the fluid flow temperature. Fig. 11(a, b, c) reveals the effect of heat source (G) on the flow fields. It is realized that the velocity and temperature profiles are enhanced with a larger value of the heat source parameter, while the reverse is the case for the concentration profile.
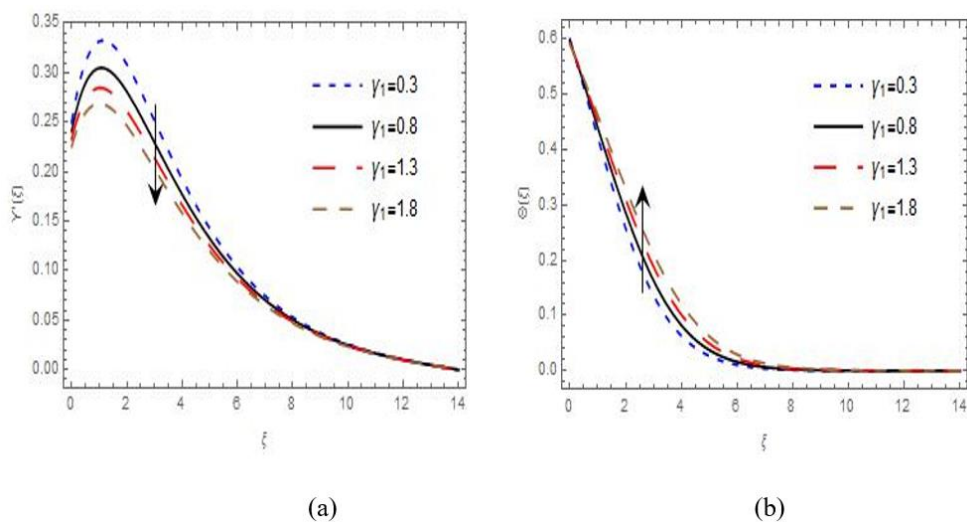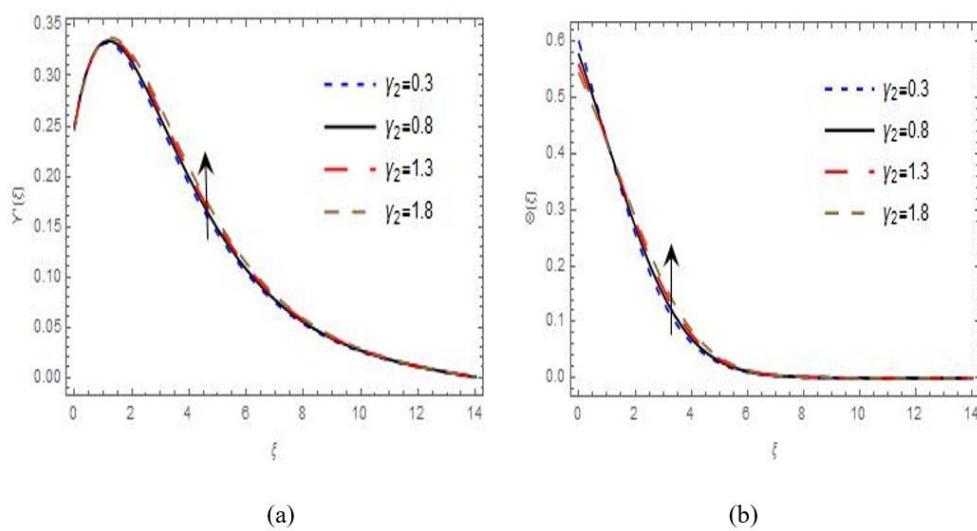
(a)

(b)

(c)
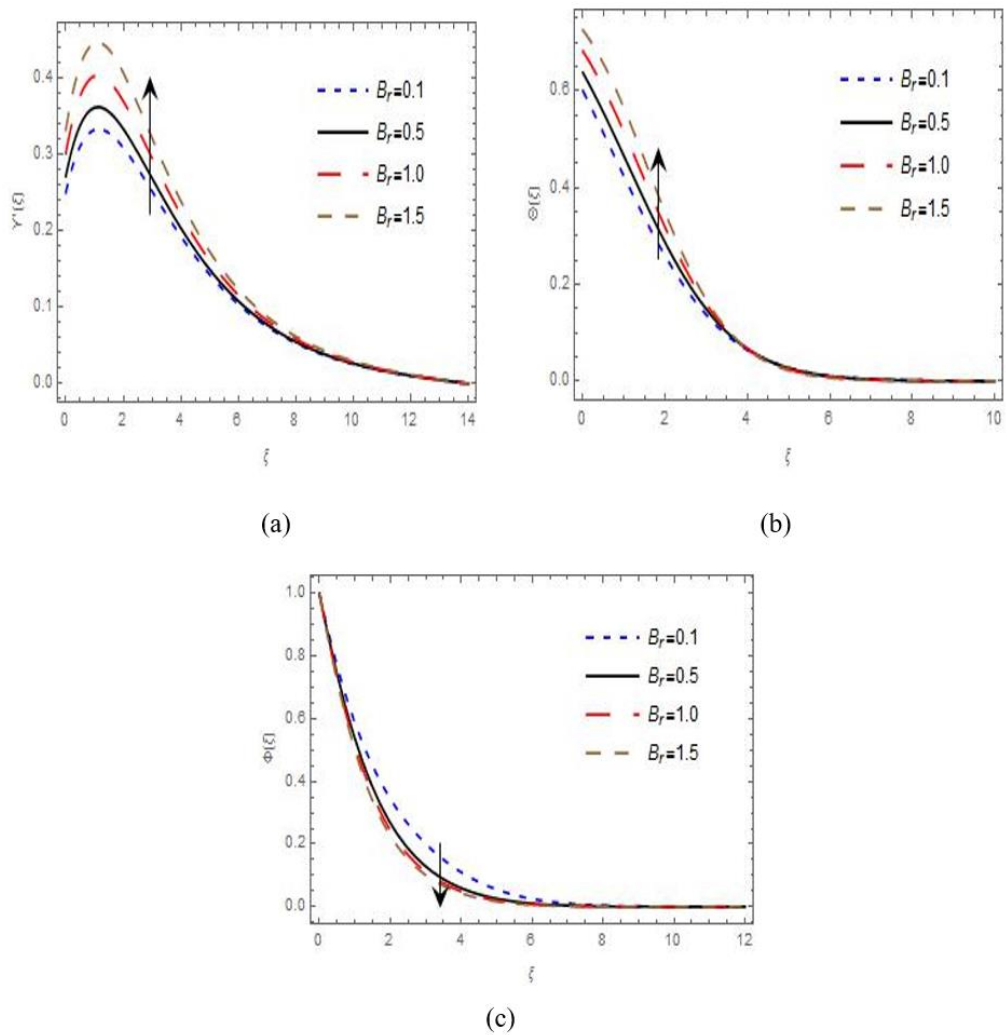
Fig. 2. Influence of T_m on (a) velocity (b) temperature (c) concentration profiles.
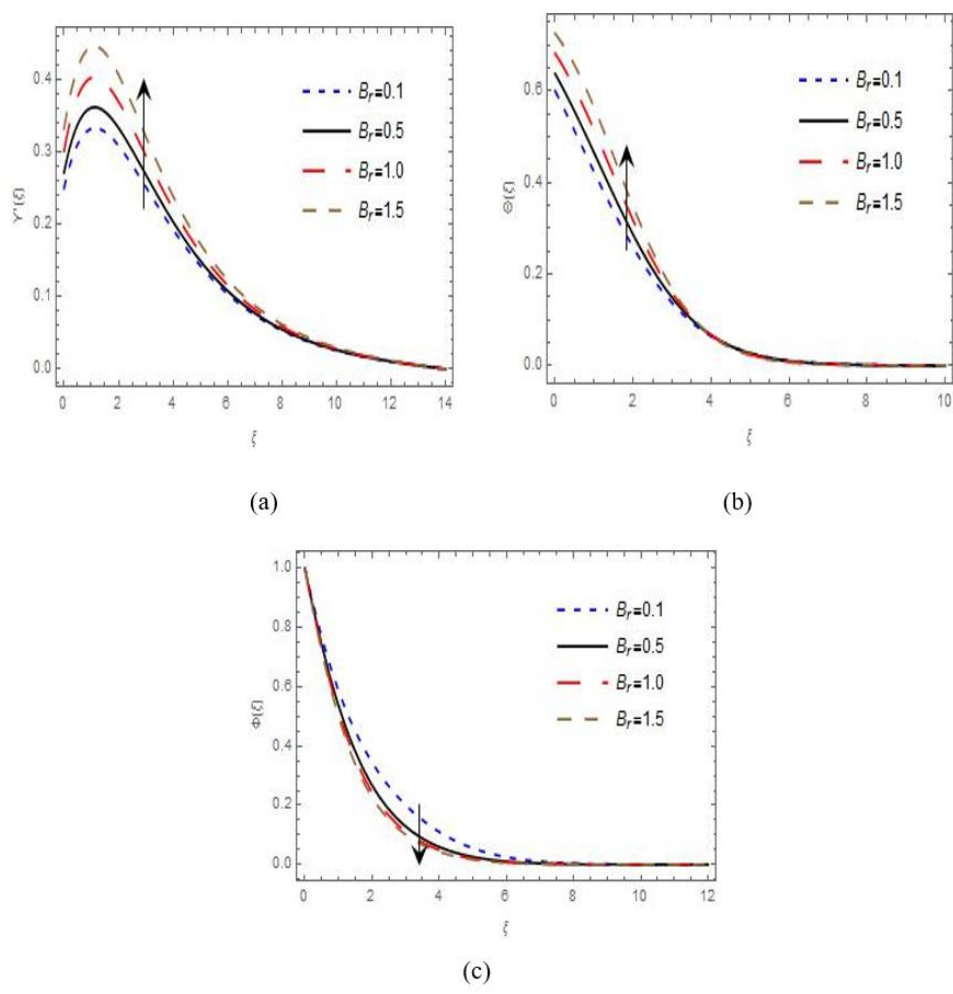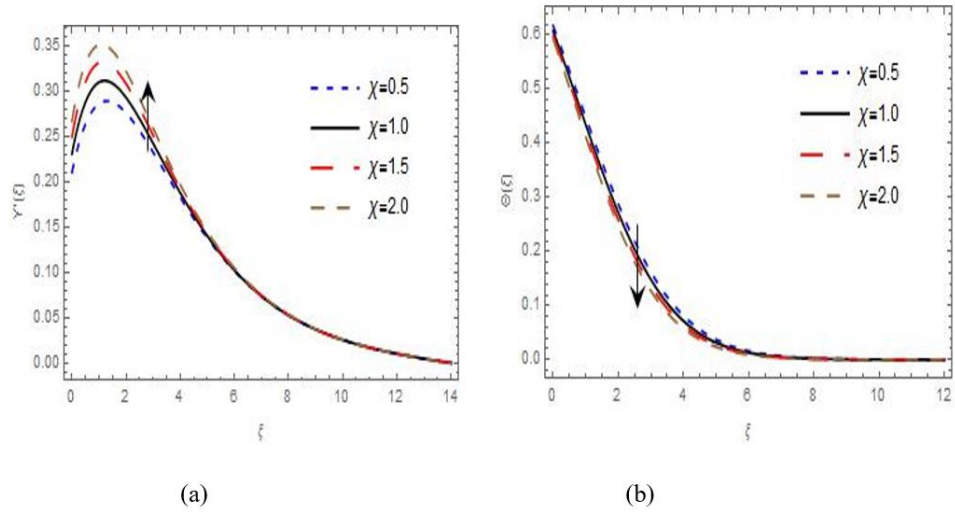
Fig. 3. Impact of B_r on (a) velocity (b) temperature (c) concentration profiles.

(a)   (b)

Fig. 4. Influence of γ_1 on (a) velocity (b) temperature profiles.

(a)   (b)

Fig. 5. Effect of γ_2 on (a) velocity (b) temperature profiles.

(a)   (b)

Fig. 6. Effect of χ on (a) velocity (b) temperature profiles.

(a)   (b)

Fig. 7. (a) Effect of ε on velocity profile (**b**) Effect of n on concentration profile.

Fig. 8. Influence of β on (a) velocity (b) temperature (c) concentration profiles.

(a)   (b)
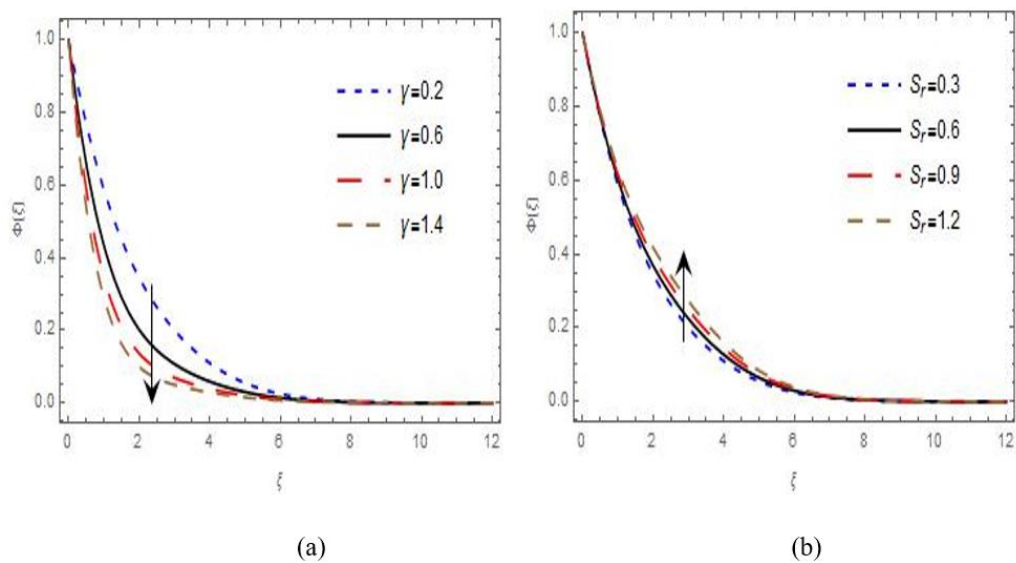
Fig. 9. Impact of (a) γ (b) Sr on concentration profile.

(a)   (b)

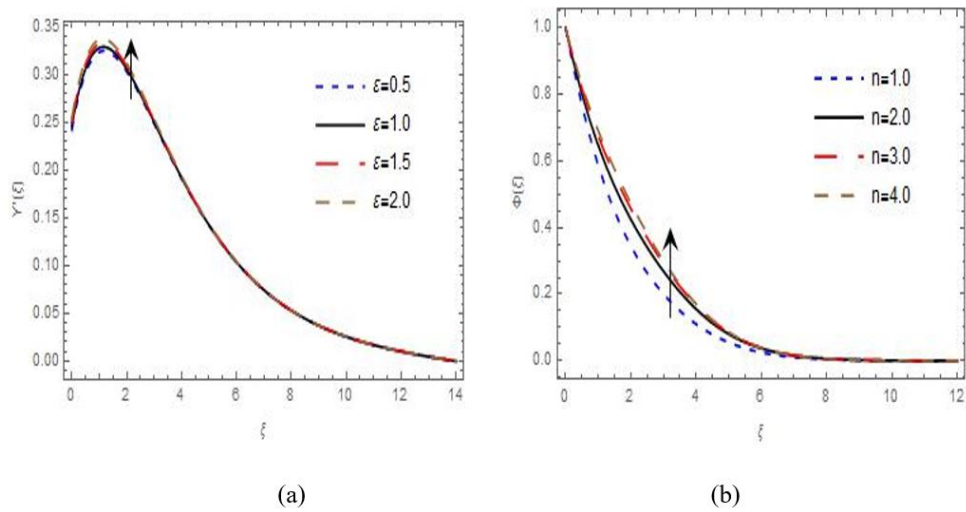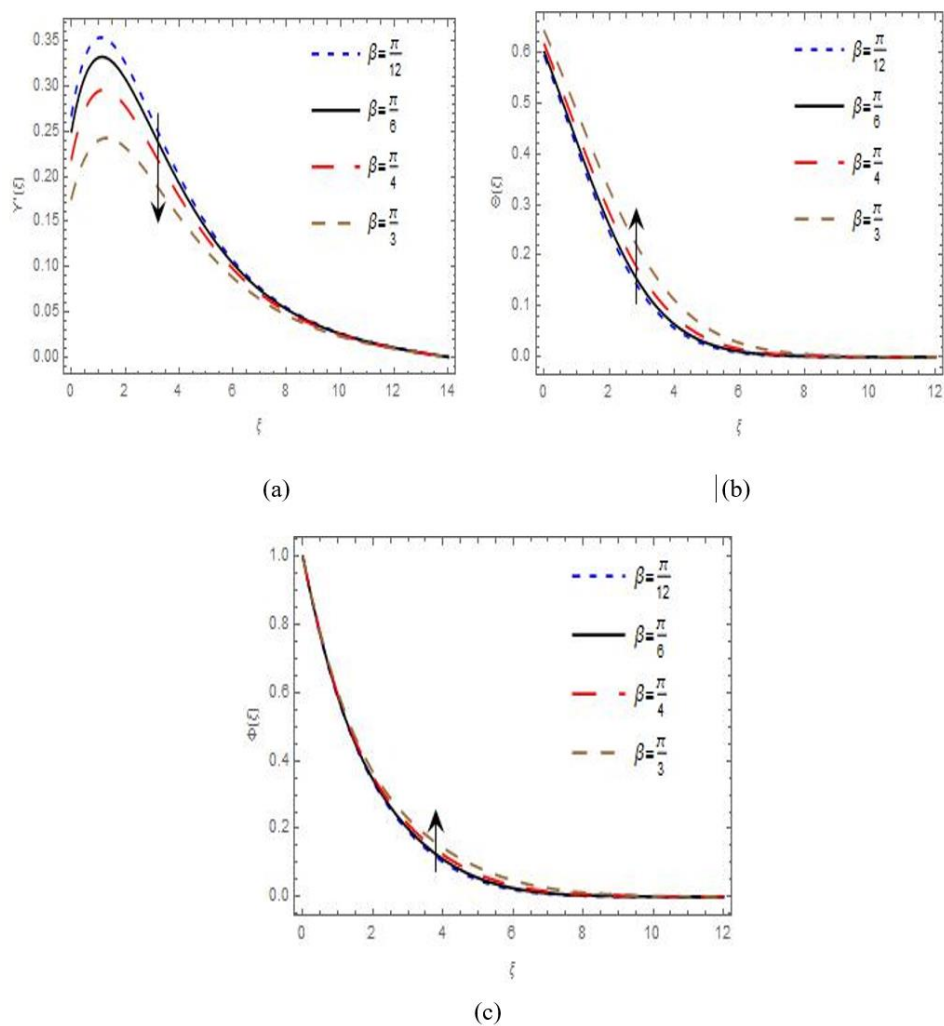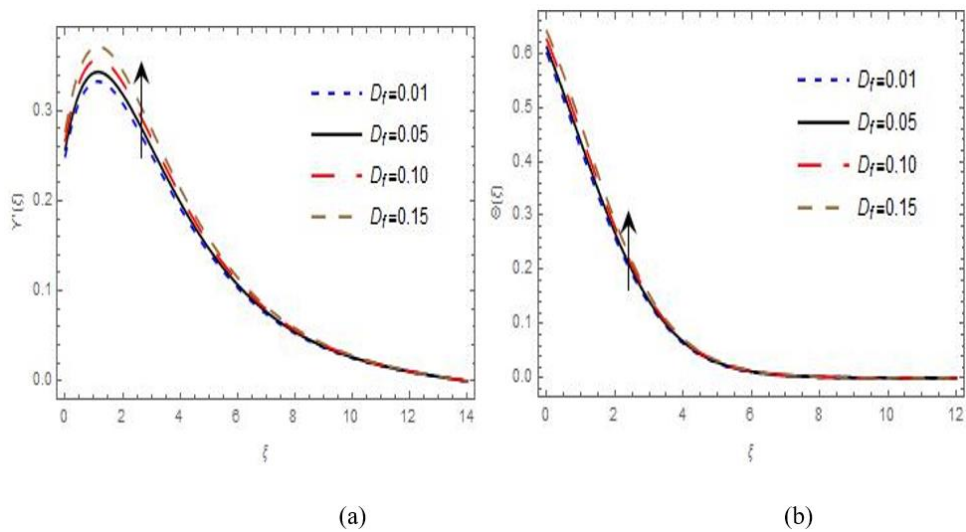**Fig. 10.** Influence of D_f on (a) velocity (b) temperature profiles.

(a)

(b)

(c)

Fig. 11. Effect of G on (a) velocity (b) temperature (c) concentration profiles.
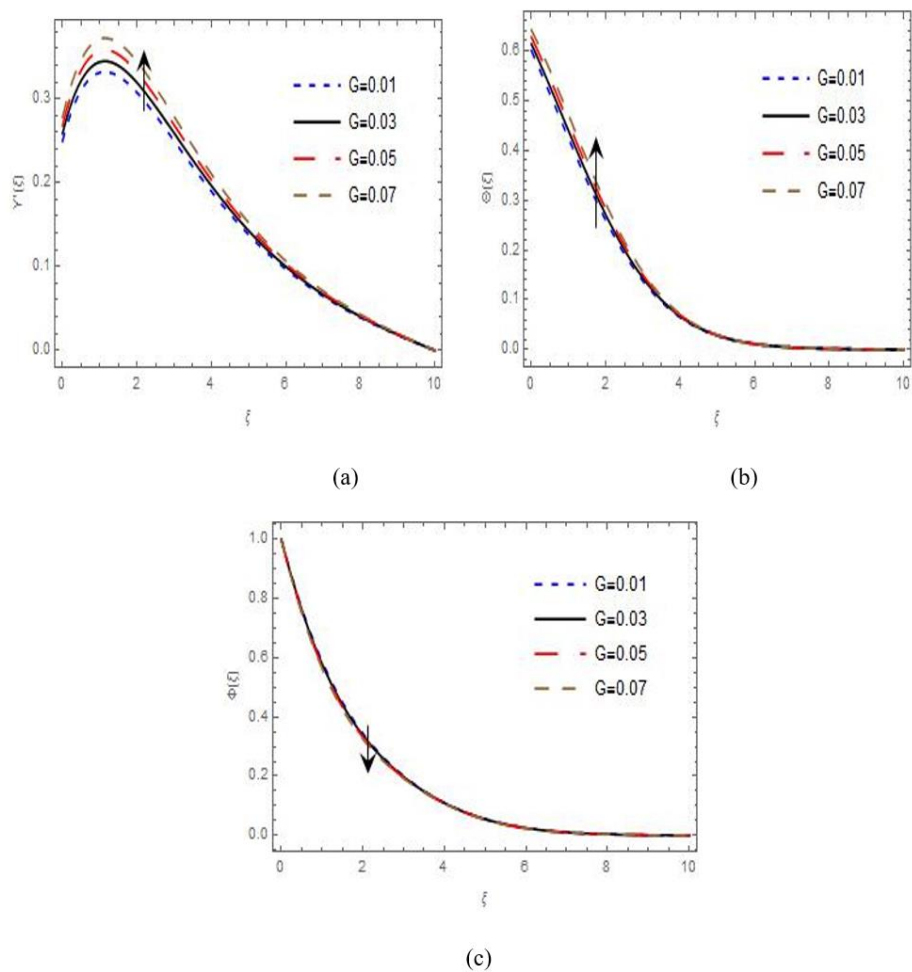
		$P_r=1$			$P_r = 5$		
B_r	$-N_r$	Uddin, et al. (2012)	Gbadeyan, et al. (2020)	Present work	Uddin, et al. (2012)	Gbadeyan, et al. (2020)	Present work
	0	0.34257	0.342575	0.34257	0.38395	0.383959	0.38375
0.1	0.2	0.33659	0.336593	0.33659	0.37734	0.377351	0.37716
	0.4	0.33012	0.330127	0.33013	0.37024	0.370246	0.37007
	0	0.2960	0.295999	0.2960	0.33288	0.332884	0.33269
0.3	0.2	0.29178	0.291778	0.29177	0.32821	0.328211	0.32804
	0.4	0.28724	0.287244	0.28724	0.32322	0.323225	0.32308

Table 1. Nusselt number comparison of the work of Gbadeyan et al. (2020) and Uddin et al. (2012) with the present work, for the values of Da= $\alpha=\infty$, $T_m=0.1$, $L_e=Bi=10$, n=1, H=R=Ec=G=D_f=S_r= Υ =B=Υ_1= Υ_2 = χ = ε =S= β=0.

D_f	S_r	G	Ec	H	R	Da	S	Bi	L_e	Υ	$-\Theta'(0)$	$-\Phi'(0)$
0.01	0.3	0.01	0.01	0.5	0.1	1.0	0.3	0.5	1.0	0.2	0.1236	0.4948
0.05											0.1176	0.5054
	0.6										0.1238	0.4850
		0.03									0.1108	0.5160
			0.05								0.1212	0.4990
				1.0							0.1236	0.4947
					0.5						0.1170	0.5014
						5.0					0.1630	0.5160
							0.6				0.1269	0.4971
								1.0			0.1557	0.4960
									3.0		0.1197	0.8957
										0.6	0.1204	0.8170

Table 2. Computational values of Nusselt and Sherwood number for various parameters of interest.

5. Conclusions

A numerical study on the effect of variable thermophysical properties on nonlinear thermal and Solutal convective flow of Casson nanofluid over an inclined surface with nth-order chemical reaction is carried out. The equations governing the fluid flow are nondimensionalized and transformed into nonlinear ordinary differential equations, using the appropriate nondimensional variables and similarity transformations, respectively. The solutions of the equations are obtained using a collocation method with the aid of assumed Legendre functions of the first kind and MATHEMATICA 11.0 software. The numerical results of the fluid flow and its characteristics are discussed for various physical parameters of interest. These are presented through graphs and tables. From the discussion of the results, the following observations are made:

1) The velocity, temperature and concentration profiles are increased with a hike in thermophoretic parameter (Tm).

2) Higher Brownian motion parameter (Br) increases the velocity and temperature profiles and slows down the concentration profile.

3) Velocity decreases and temperature increases with a hike in variable viscosity (γ1).

4) A rise in variable thermal conductivity (γ2) and heat source parameter (G) accelerates both velocity and temperature and suppresses the fluid concentration profiles.

5) A larger value of inclination angle (β) reduces the velocity and increases the temperature profiles.

6) The velocity and temperature fields increase with (Df).

7) The velocity increases and temperature decreases with a rise in nonlinear thermal convection parameter (χ). Higher value of nonlinear Solutal convection parameter (ε) also gives rise to velocity.

8) The concentration profile is enhanced with Soret (Sr) and the order of chemical reaction (n) and suppressed with a hike in chemical reaction parameter (γ).

Nomenclature

Pr   Prandtl number

Q   dimensional internal heat source

D_T thermophoresis diffusion coefficient

D_m Brownian motion coefficient

K_p Porous medium permeability

ρ_f fluid density

$\mathcal{K}$ thermal conductivity

τ heat capacity of nanoparticle to the base fluid ratio

$h_f(\overline{x})$ heat transfer coefficient

Λ_0, Λ_2 linear thermal, Solutal expansion coefficient respectively

Λ_1, Λ_3 nonlinear thermal, Solutal expansion coefficient respectively

$\overline{u}, \overline{v}$ fluid velocity in the $\overline{x}, \overline{y}$ direction respectively

g   acceleration due to gravity

B_r Brownian motion parameter

G   heat source parameter

C_p specific heat capacity

Ra   Rayleigh number

L_e Lewis number

D_f Dufour parameter

S_r Soret parameter

T_m Thermophoresis parameter

D_a Darcy number

C_S absorption susceptibility

ρ_p nanofluid density

T   fluid temperature

D_B Brownian diffusion coefficient

γ_1, γ_2 variable viscosity, thermal conductivity parameter

μ Viscosity constant coefficient

k_0 thermal diffusion ratio

b^* Forchheimer's coefficient

χ, ε nonlinear thermal, Solital convection parameter

k   constant rate of chemical reaction

S_1 slip constant

n   order of chemical reaction

γ   chemical reaction parameter

B_0 constant magnetic field

σ_0 constant electricity conductivity

α   Casson parameter

β   inclination angle

σ   variable electric conductivity

S   slip parameter

H   magnetic field parameter

Ec   Eckert number

Nr   buoyancy ratio

R   radiation parameter

B   porosity parameter

Bi   Biot number

References

Akolade MT, Adeosun AT and Olabode JO (2021a). Influence of thermophysical features on MHD squeezed flow of dissipative Casson fluid with chemical reaction and radiative effects. J. Appl. Comp. Mech. Doi: 10.22055/jacm.2020.34909.2508.

Akolade MT, Idowu AS, Adeosun AT (2021b). Multislip and Soret-Dufour influence on nonlinear convection flow of MHD dissipative Casson fluid over a slendering stretching sheet with generalized heat flux phenomenon. Heat. Trans. Res., 50(4): 3913-3933.

Animasaun IL (2015). Effect of thermophoresis, variable viscosity and thermal conductivity on free convective heat and mass transfer of non-darcian MHD dissipative Casson fluid flow with suction and nth order chemical reaction. Journal of Nigeria mathematical society, Vol. 34, pp 11-31.

Aysun G and Salih Y (2013). Legendre collocation method for solving nonlinear differential equations. Math. Comput. Appl. 18(3), 521-530 (2013).

Buogioro J (2006). Convective transport in nanofluids. J. Heat trans. TASME 2006:128:240-250

Chaoyang W. and Chuanjing T.U. (1989). Boundary layer flow and heat transfer of non-Newtonian fluid in porous medium. Int. J. Heat fluid flow. Vol.10, No.2, pp.160-165.

Daniel YS, Aziz ZA, Ismail Z, Salah F (2017). Thermal radiation on unsteady electrical MHD flow of nanofluid over stretching sheet with chemical reaction. J. King Saud Univ. Sci. 2017; 31:804-812.

Faisal MB, Kohilavani N, Ehtshan H, Zaffar M, Swati M, Roslinda N, Anuar J, Dumitru B, Kottakkaran SN and Ilyas K (2021). Unsteady nano-bioconvective channel flow with effect of nth order chemical reaction. Published by De Gruyter, Open physics (2020); 18: 1011-1024

Gbadeyan JA, Oyekunle TL, Fasogbon PF and Abubakar JU (2018). Soret and Dufour effects on heat and mass transfer in chemically reacting MHD flow through a wavy channel. Journal of Taibah university for Sci. Vol. 12, No.5, pp. 631-651.

Gbadeyan JA, Titiloye EO, Adeosun AT, (2020). Effect of variable thermal conductivity and viscosity on Casson nanofluid flow with convective heating and velocity slip. Helyon, 1(6): e0307b.

Gupta S, Kumar D, Singh J. (2018). MHD mixed convective stagnation point flow and heat transfer of an incompressible nanofluid over inclined stretching sheet with chemical reaction and radiation. Int. J. Heat Mass transf. 2018; 118:378-387.

Hayat T, Awais M, Qasim M, Hendi AA (2011). Effect of mass transfer on the stagnation point of flow of an upper-convected Maxwell (UCM)fluid. Int. J. Heat and Mass transfer. 2011;54: 3777-3782.

Hayat T, Khan MI, Farooq M, Gull N and Alsaedi A. (2016). Unsteady three-dimensional mixed convection flow with variable viscosity and thermal conductivity. J. Molecular Liq.,223:1297-1310.

Ibrahim SM, Lorenzini G, Kumar PV and Raju CSK (2017). Influence of chemical reaction and heat store on dissipative MHD mixed convection flow of a Casson nanofluid over a nonlinear permeable stretching sheet. Int. J. Heat Mass Transf. 111:346-355

Idowu AS and Falodun BO (2020). Variable thermal conductivity and viscosity effects on non-Newtonian fluids flow through a vertical porous plate under Soret-Dufour influence. Math. Comp. Simul. 177:358-384

Idowu AS, Akolade MT, Oyekunle TL, and Abubakar JU (2021). Nonlinear convection flow of dissipative Casson nanofluid through an inclined annular microchannel with a porous medium. Heat Trans. Res., 50(4): 3388-3406.

Jawad R, Azizah M and Zurn O (2016). Multiple solution of mixed convective MHD Casson fluid flow in a channel. Journal of Applied Mathematics. Vol. 2016, pp 1-10.

Jawali CU and Chamkha AJ (2015). Combined effect of variable viscosity and thermal conductivity on free convection flow of a viscous fluid in a vertical channel. Int. J. Num. Meth. Heat flow. 26(1): 18-39

Kumar R and Sood S (2016). Interaction of magnetic field and nonlinear convection in the stagnation point flow over a shrinking sheet. J. Eng. http://dx.doi.org/10.1155/2016/6752520.

Lognathan P, Iranian D, Ganesan P. (2011). Effect of chemical reaction on unsteady free convective heat and mass transfer flow past a vertical plate with variable viscosity and thermal conductivity. Eur. J. Sci. Res. 2011; 59(31): 403-416.

Malik MY, Jamil H, Salahuddin T, Bilal S, Rehman KU, Mustafa Z. (2016). Mixed convection dissipative viscous fluid flow over a rotating cone by way variable viscosity and thermal conductivity. Res. Phy., 6:1126-1135

Nagendramma V, Raju CSK, Mallikanjuna B, Shehzad SA, and Leelarathnam A. (2018). 3D Casson nanofluid flow over slendering surface in a suspension of gyrotactic microorganisms with cattano-christov heat flux. Appl. Math. Mech, 39:623-628

Olagunju AS, Joseph FL, Raji MT (2013). Comparative study of the effect of different collocation Points on Legendre-collocation method of solving second-order boundry value problems. IQSR J. Math 7(2), 35-41 (2013)

Oyekunle TL, Akolade MT and Agunbiade SA (2021). Thermal-diffusion and Diffusion-thermo effects on heat and mass transfer in chemically reacting MHD Casson nanofluid with viscous dissipation. Int. J. Application and Applied Mathematics. Vol.16, issue 1(2021), pp.705-723.

Patil PM and Kulkami M (2019). Nonlinear mixed convective nanofluid flow along moving vertical rough plate. Revista Mexican fisica. 66(2):135-161

Raju AB, Raju GSS and Mallikajuna B (2017). Unsteady quadratic convective flow of a rotating non-Newton fluid over a rotating cone in a non-porous medium. Int. J Adv. Res. Comput. Sci. 8(7) 68-72.

Raju AB, Raju GSS, Mallikanjuna B, Raju CSK (2018). Effect of nonlinear convection and variable properties on darcy flow of non-Newtonian fluid over a rotating cone. Int. J. Res. Eng. Appl. Manag. 4(2) 586-594

Salawu SO and Dada MS (2016). Radiative heat transfer of variable viscosity and thermal conductivity effect on inclined magnetic field with dissipation in a non Darcian medium. J. Nig. Math. Soc., 35(1), (2016) 93-106.

Shah S, Hussain S, Sagheer M (2018). Impacts of variable thermal conductivity on stagnation point boundary layer flow past a Riga plate with variable thickness using generalized Fourier's law. Results Phys. 2018; 9:303-312

Uddin MJ, Khan WA, and Ismail AI (2012). MHD free convective boundary layer flow of a nanofluid past a flat vertical plate with Newtonian heating boundary condition, PloS ONE 7, e49499

Umavathi JC, Sheremet MA and Mohiuddin S (2017). Combined effects of variable viscosity and thermal conductivity on mixed convection flow of a viscous fluid in a vertical channel in the presence of first order chemical reaction. European J. Mech. B/fluid, 58: 98-108.

Upadhya SM, Raju CSK, and Saleem S. and Alderremy AA (2018b). Modified Fourier heat flux on MHD flow over stretched cylinder filled with dust, Graphene and silver nanoparticles. Results Phy, 9:1373-1385

Upadhya SM, Raju CSK and Saleem S (2018a). Nonlinear unsteady convection on micro and nanofluid with catton-christov heat flux. Result Phy. 9:779-786